ADVANCED ENERGY & SUSTAINABILITY RESEARCH
www.advenergysustres.com

Downshifting Encapsulant: Optical Simulation Evaluation of the Solution to Ultraviolet-Induced Degradation in Silicon Heterojunction Solar Cells

Binbin Xu, Karsten Bittkau, Alexander Eberst, Kai Zhang, Yanxin Liu, Jinli Yang, Weiyuan Duan, Muhammad Ainul Yaqin, Vladimir Smirnov, Chunlan Zhou, Wenjing Wang, Xiaohua Xu, Andreas Lambertz, Uwe Rau, and Kaining Ding**

Ultraviolet (UV)-induced degradation (UVID) poses a significant challenge for the prospective mass production of silicon heterojunction (SHJ) solar cells, known for their high efficiency. In this study, the magnified impact of UV radiation when employing a silicon carbide (SiC)-based transparent passivating contact (TPC) on the front side of SHJ solar cells is reported. A reduction in open-circuit voltage (V_{OC}), short-circuit current (J_{SC}), and fill factor of 12%, 6%, and 11%, respectively, is observed after UV exposure. Conventional UVID mitigation measures, UV-blocking encapsulation, are assessed through single-cell TPC laminates, revealing an unavoidable tradeoff between current loss and UVID. Alternatively, the utilization of ultraviolet-downshifting (UV-DS) encapsulants is proposed to convert UV radiation into the visible light spectrum. An optical simulation method, conducted via OPAL2, is presented to evaluate UV-DS encapsulants for diminishing UVID in SHJ solar cells with different front contacts. A simple methodology is proposed to mimic the optical property of UV-DS encapsulants. In the simulation results, additional current gains of up to 0.33 mA cm^{-2} achievable with suitable UV-DS encapsulants are highlighted. The factors related to the UV-DS effects are evaluated and the optimization pathway for UV-DS encapsulants is elucidated.

1. Introduction

The prospect of achieving a zero-carbon footprint continually drives the expansion of the share of photovoltaic (PV) in the global energy supply, thus accelerating the deployment of solar modules worldwide.[1] This substantial demand has drawn significant attention to advanced high-efficiency crystalline silicon (c-Si) solar cell technologies. Among the promising candidates, silicon heterojunction (SHJ) technology stands out due to its exceptional passivation, lean and low-temperature processing, low-temperature coefficient, and advantageous bifacial structure.[2,3] Collaborative efforts have showcased the remarkable potential of SHJ technology, which currently holds the record efficiency for single-junction solar cells in a front/back-contacted configuration.[4] The rising number of industrial mass-production plants for SHJ solar cells and modules further underscores its trajectory toward becoming a mainstream PV technology. Nevertheless, to remain competitive with other technologies, continued innovation is essential for further enhancing the efficiency of mass-produced SHJ solar cells. In the classical SHJ architecture, hydrogenated amorphous silicon (a-Si:H) serves the dual purpose of passivating the unsaturated silicon wafer surface and collecting photo-generated carriers. However, it was found that the parasitic absorption in the a-Si:H layers results in the lower short-circuit current density (J_{SC}) of SHJ

B. Xu, K. Bittkau, A. Eberst, K. Zhang, Y. Liu, W. Duan, M. A. Yaqin, V. Smirnov, A. Lambertz, U. Rau, K. Ding
IMD-3 Photovoltaics
Forschungszentrum Jülich GmbH
52428 Jülich, Germany
E-mail: b.xu@fz-juelich.de; k.ding@fz-juelich.de

The ORCID identification number(s) for the author(s) of this article can be found under https://doi.org/10.1002/aesr.202400227.

DOI: 10.1002/aesr.202400227

B. Xu, A. Eberst, K. Zhang, Y. Liu, M. A. Yaqin, U. Rau
Jülich-Aachen Research Alliance (JARA-Energy) and Faculty of Electrical Engineering and Information Technology
RWTH Aachen University
Schinkelstr. 2, 52062 Aachen, Germany

J. Yang, C. Zhou, X. Xu
Institute of Electrical Engineering
Chinese Academy of Sciences
100190 Beijing, China

J. Yang, C. Zhou, X. Xu
University of Chinese Academy of Sciences
100190 Beijing, China

W. Wang, X. Xu
Anhui Huasun Energy Co., Ltd.
242000 Xuancheng, China

solar cells compared with its homojunction counterpart, which is regarded as one of the bottlenecks for approaching its efficiency to the theoretical limit.[2–5]

Many research groups propose to replace a-Si:H with other Si-based materials, which typically show an optical bandgap (E_{04}) $\geq$2.0 eV, higher than a-Si:H. For instance, studies suggest that substituting the doped layer, n-type a-Si:H ($E_{04} \approx 1.86$ eV), with hydrogenated nanocrystalline silicon (nc-Si:H) ($E_{04} \approx 2.0$ eV)[6] or hydrogenated nanocrystalline silicon oxide (nc-SiO_x:H) (E_{04}: 1.9–2.95 eV)[7] can notably minimize the parasitic absorption. A record cell efficiency has been achieved with a front contact comprising an nc-SiO_x:H/nc-Si:H stack.[5] However, despite the advancements, all these cell structures still rely on intrinsic hydrogenated amorphous silicon (a-Si:H(i)) for sufficient passivation, which undermines the effort to minimize parasitic absorption losses. In our previous research, we introduced a front transparent passivating contact (TPC) structure that combines the large-bandgap n-type hydrogenated nanocrystalline silicon carbide (nc-SiC:H(n)) with a wet-chemically prepared SiO_x tunneling layer, demonstrating significant J_{SC} gains.[5]

The durability of SHJ solar cells and modules is pivotal to their technological success. Recent investigations into ultraviolet-induced degradation (UVID) present a new challenge along the path to success of SHJ technology. Research by Sinha et al. highlights that SHJ solar cells, particularly those without encapsulation, are notably affected by UV radiation compared to other contemporary c-Si solar cells.[8] After UV exposure, the open-circuit voltage (V_{OC}) and fill factor (FF) of SHJ cells decreases significantly, probably due to UV-induced hydrogen effusion near the interface of a-Si:H/c-Si. It is worth noting that this study focuses on front-junction SHJ cells with the a-Si:H(p)/a-Si:H(i) stack on the front side. A similar reduction of V_{OC} and FF was observed in the study by Ye et al. The investigation into different a-Si:H layers and cell precursors shows that high-energy UV photons can break Si—H bonds in all types of a-Si:H layers and increase the defect density at the a-Si:H/c-Si interface.[9] Measures to mitigate UVID have been widely discussed among researchers, which can be broadly categorized as UV blocking and UV exploitation. Blocking UV by encapsulation is a more common strategy, which involves incorporating UV absorbers into the encapsulant formulation to tailor its transmittance.[8,9] The SHJ modules encapsulated with ethylene vinyl acetate (EVA), which have a UV cutoff of 380 nm, have demonstrated their resistance to UV degradation in both the accelerated UV exposure test and the outdoor test.[9] However, UV absorbers can prompt the formation of yellow chromophores in the encapsulant, impairing its transmittance and leading to photogenerated current loss.[10] On the contrary, utilizing UV light through down-conversion (DC) or downshifting (DS) processes is gaining attention as a promising alternative.[11] Yang et al. proposed a novel UV-DC encapsulating film capable of converting visible light with high quantum efficiencies.[12] The application of this film to the encapsulation of SHJ solar cells shows extra power gain. In addition, the deposition of large-bandgap (blue) luminescent DS quantum dots films on the surface of SHJ solar cells enabled color-patterned solar cells with power conversion efficiency exceeding 23.5%.[13] By introducing localized-surface-plasmon-resonance-enhanced DS nanophosphors on top of SHJ solar cells, the efficiency degradation under UV irradiation was decreased by about 0.54% in relative terms.[14] DS typically denotes a single-photon process with quantum efficiencies not exceeding 100%,[15,16] to which the work presented later mainly relates. The aforementioned literature verified the feasibility of using DS layers to mitigate or avoid UVID, but most of the work was driven by a relatively vague goal of converting UV photons into long wavelength photons. The key question, to which wavelength the converted UV photons can provide the greatest gain for SHJ solar cells, was still not answered. The experiments aiming to answer this question would rather be a complex process, given the complexity of developing DS materials with different UV-converting properties. Here, our approach is to use numerical simulations, which can speed up the investigation and successfully address the discussed points. Up to now, several basic models have been used for treating the DS layers, like ray tracing[17] or the spectral transfer matrix formalism.[18] In the case of a work investigating luminescent DS layers for organic solar cells, a 3D ray-tracing model was developed to simulate the DS layer based on phosphor particles. A novel effective approach was applied to the ray-tracing model, the simulation results fitted the experimental data very well and successfully predicted the gain with the DS layer by integrating it into an optical simulator combined ray optics/wave optics model.[19] Rothemund proposed a simplified luminescent DS model which can extract the total DS efficiency from the experimental quantum efficiency spectra.[20] A simulation based on this model showed good agreement with the experimental data for investigating nanostructured organosilicon luminophores in DS layers.[21]

In this study, we first aim to experimentally show that UVID could be a common phenomenon in c-Si solar cells utilizing SHJ technology, regardless of which the hydrogenated front passivating contact structures are applied. The performance of SHJ and TPC solar cells was examined after UV exposure. UVID was observed in both cells. However, only a reduction in V_{OC} was observed in SHJ cells, but substantial V_{OC} and FF losses were observed in TPC cells. A significant decrease in the J_{SC} of TPC cells was also observed, which indicates that the application prospect of the TPC structure to generate higher currents could be challenging. To examine potential solutions, we evaluated measures to mitigate UVID at the module level from an optical perspective, discovering a tradeoff between current loss and UVID that normal encapsulant strategies were nearly unable to solve. Therefore, we propose to use DS encapsulants to modulate the spectrum illuminating the solar cells, thereby converting harmful UV light into visible light that can be beneficially utilized by the solar cells. A general evaluation, not limited to TPC but to various SHJ solar cells with different front contacts, was performed by a simplified optical model mimicking DS encapsulants and subsequent OPAL2 simulations. The effects of DS encapsulation, factors correlated with DS effects, and a potential optimization pathway are discussed.

2. UVID in SHJ and TPC Solar Cells

Figure 1a illustrates the configurations of the c-Si solar cells utilized in UV exposure experiments, employing two types of front contacts. The SHJ solar cells utilize the standard a-Si:H(n)/a-Si:H(i) stack on the front side, aiming to evaluate UVID in SHJ

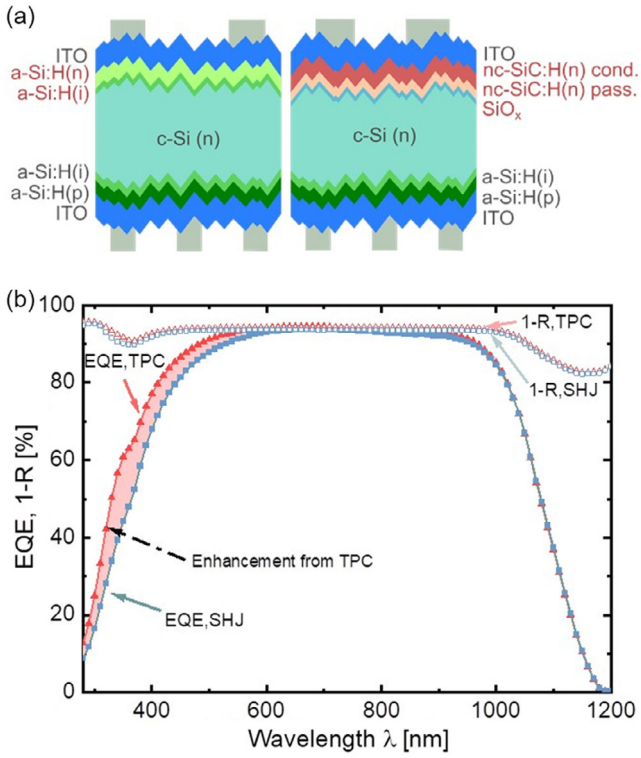

Figure 1. a) Sketch of bifacial silicon heterojunction (SHJ, left) and transparent passivating contact (TPC, right) crystalline silicon solar cells. b) The external quantum efficiency (EQE) and reflectance spectra of SHJ and TPC solar cells.

solar cells and make comparisons with findings reported by other research groups.[9] Reducing parasitic absorption from passivating contacts is a key development direction for SHJ solar cells. The TPC concept has emerged as a potential solution to address this issue. Therefore, the performance of c-Si solar cells using TPC under constant UV irradiation is also of interest. The TPC structure in this study consists of nc-SiC:H(n) prepared by hot-wire chemical vapor deposition (HWCVD) on nc-SiC:H(n).[5] By depositing wide-bandgap materials on the front side, with a SiO_x tunneling passivating layer, the J_{SC} of TPC solar cells can be significantly enhanced. The external quantum efficiency (EQE) and reflectance (R) spectral response, shown in Figure 1b, also confirms this improvement. The integrated current (J_{EQE}) calculated from the EQE response is 37.79 mA cm^{-2} for the SHJ cell and 38.56 mA cm^{-2} for the TPC cell, indicating a current gain of 0.77 mA cm^{-2} due to the TPC structure. The optical losses resulting from the reflection are similar for both types of solar cells, but the EQE spectrum of the TPC cell suggests that the enhancement primarily arises from light with shorter wavelength, particularly in the UV range. In other words, a more transparent front contact allows more UV light to be absorbed by the c-Si substrate. This behavior attracts our attention and sparks further interest in investigating the effects of UV light on TPC solar cells.

Experiments were conducted on both SHJ and TPC solar cells to assess the effects of UV exposure. Three distinct conditions were established to isolate the effects of dark degradation, UV chamber temperature, and UVID during the UV exposure process. To ensure the accuracy of the evaluation, the performance parameters of the solar cells were normalized by dividing the value after UV exposure by the initial value. Given the widespread reports linking UVID to changes in V_{OC} and FF,[8,9] our primary focus was directed toward analyzing these two parameters. **Figure 2** illustrates the performance of SHJ solar cells and TPC solar cells in relation to the different testing conditions. V_{OC} losses due to UV irradiation are also observed in our experiments, as depicted in Figure 2a. The normalized V_{OC} of SHJ drops to 0.99 after a UV exposure of 60 kWh m^{-2}, which means an absolute loss of about 6 mV. It is consistent with the level reported by other researchers.[9] Surprisingly, TPC cells exhibited a substantial reduction of normalized V_{OC} to 0.88, indicating a loss of ≈92.75 mV. This significant change in V_{OC} suggests that a dramatic change may take place at the interface between SiO_x and c-Si in the TPC structure, considering that more UV light can pass the passivating film and reach the interface.[22] In contrast, the microstructure of nc-SiC:H(n) or SiO_x may also be altered. The control samples show no change when stored in the dark or treated with heat but not UV irradiation. This suggests that most of the change could be induced by UV light. Ye et al. discovered that ultraviolet A (UVA, 320–400 nm) light can provide enough energy to disrupt Si—H bonds at the interface and a-Si:H films of SHJ cells.[9] A similar reason could presumably lead to the breakage of Si—H bonds in the TPC contact, followed by the incubation of defects driving passivation degradation. This implies that any cell structure that relies on hydrogen for passivation may be susceptible to UVID in passivation.

Contrary to observations in other studies, Figure 2b reveals almost no difference in the normalized FF of SHJ cells after all three conditions, consistent with the nearly unchanged pseudo *FF* (pFF) and series resistance (R_S) depicted in Figure 2c,d, respectively. There are several possible reasons for explaining this. On the one hand, differences in a-Si:H materials or stacks used by different investigators may lead to different behavior of FF under UV exposure. For example, the a-Si:H(i) layer used in contemporary SHJ cells is composed of a porous sublayer and an overlying dense sublayer.[23] Different investigators might use different stacks and deposition conditions, giving different microstructures. It can be expected that different microstructures may lead to different degradation behaviors. Maybe in our case a longer exposure is required to show an observable change in FF. On the other hand, the setting of the UV exposure experiments may also affect the behavior of FF. To mimic the actual field operation temperature of solar cells, the temperature of the UV chamber was set at 60 °C, which is 20 °C higher than that used in ref. [9]. In our ongoing investigation, we observed a correlation between UVID and the temperature of the UV chamber, but the detailed mechanism needs further clarification. However, UV light again shows a clear effect on the degradation of the FF of TPC solar cells. Figure 2b demonstrates a huge reduction in the normalized FF of TPC cells in the case of UV irradiation. The normalized FF drops to 0.94, whereas there is no change observed for the other two conditions. An examination of FF-related parameters indicates a significant increase in R_S in the UV-treated TPC cells, although there is a slight boost in the normalized pFF. It can therefore be concluded that the FF loss in the TPC cells is driven by the R_S. The reduction in J_{SC} cannot be observed in the SHJ cells, but the J_{SC} of TPC cells

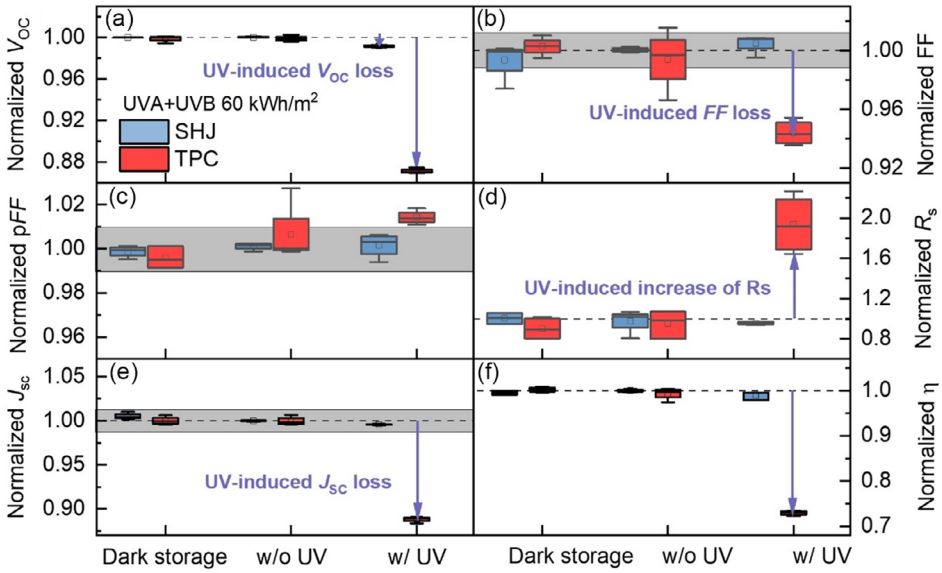

Figure 2. a) normalized V_{OC}, b) normalized FF, c) normalized pFF, d) normalized R_S, e) normalized J_{SC}, and f) normalized efficiency (η) of silicon heterojunction (SHJ) and transparent passivating contact (TPC) solar cells at different conditions of the UV exposure experiments. Dark storage means keeping the reference samples in the N_2 box in the dark environment. Without UV means loading the samples in the UV chamber at 60 °C but switching off the UV light source. With UV condition is the accelerated UV exposure test condition at 60 °C. The gray area represents the error range that can be considered as no change in a particular parameter.

is reduced to 0.89 after UV exposure, as shown in Figure 2e. This is a new phenomenon which has not been observed in solar cells utilizing SHJ technology with a-Si:H front layers. One hypothesis is that prolonged UV exposure has a major effect on both the interface and the microstructure of nc-SiC:H, which could be reflected as increased absorption or low-efficient carrier transport. All of these UVID effects lead to a dramatically reduction in efficiency (η) of TPC cells, which is decreased to 0.73 of the initial value, as shown in Figure 2f.

The observation of undesirable UVID in SiC-based TPC solar cells marks a novel phenomenon, but the detailed underlying mechanism remains to be clarified. Further material and device characterization to elucidate this mechanism is underway. In conclusion, UVID is evident in both SHJ solar cells with conventional a-Si:H contact layers and those employing advanced, highly TPC layers. Therefore, a trade-off between less parasitic absorption and stability issues leading to serious UVID is required. Solutions to mitigate the UVID need to be proposed and verified.

3. Current Losses Resulting from UV-Cutoff Encapsulation

The PV community tends to address UVID at the module level by adapting the encapsulant materials to block the UV light. For instance, thermoplastic olefin (TPO), as utilized in this context, can achieve a UV-cutoff wavelength of around 380 nm, effectively blocking most UV photons from reaching the surface of the solar cells. However, UV absorbers present in encapsulant materials like TPO may pose durability issue when exposed to UV irradiation.[10,24] Furthermore, employing UV-cutoff encapsulants inevitably results in current losses, as UV photons are no longer utilized. The impact would become more pronounced in modules composed of TPC solar cells, as they have higher transparency, as previously shown. As mentioned earlier, the current enhancement of TPC primarily occurs in the UV range, implying that UV-cutoff encapsulation could potentially diminish or eliminate this enhancement.

To quantify the current losses, we fabricated various glass/back sheet laminates using TPC solar cells, with the distinction being the front encapsulant material. The UV-cutoff laminate incorporates TPO on the front side. Conversely, for the UV-transmitting laminate, we utilized a multilayer encapsulant known as EPE, which combines the advantages of EVA and polyolefin (PO).[12] **Figure 3**a illustrates the EQE comparison between these different laminates, with the EQE of the encapsulated TPC cell included as a reference. When using EPE as the encapsulant, a minor current loss is observed in the UV range, spanning from 280 to 400 nm. In contrast, since the UV-cutoff wavelength of TPO is 380 nm, it can be assumed that there is no current generated by photons with wavelengths shorter than 380 nm. Compared to the bare TPC cell, current losses even occur in the wavelength range from 380 to 400 nm, compared to the TPC cell. This demonstrates that the current gain derived from the special TPC structure will diminish if a UV-cutoff encapsulant is applied to the front side of the module. An estimation of the current loss in the UV range was calculated by comparing the integrated currents of the spectral response data from 280 to 480 nm, denoted as J_{EQE_UV}. The integrated current for the EPE laminate and the TPO laminate is 0.86 and 0.33 mA cm^{-2}, respectively. This indicates that the current loss resulting from UV-cutoff encapsulation is ≈0.53 mA cm^{-2}, which offsets most of the gain from the cell design in terms of reducing parasitic

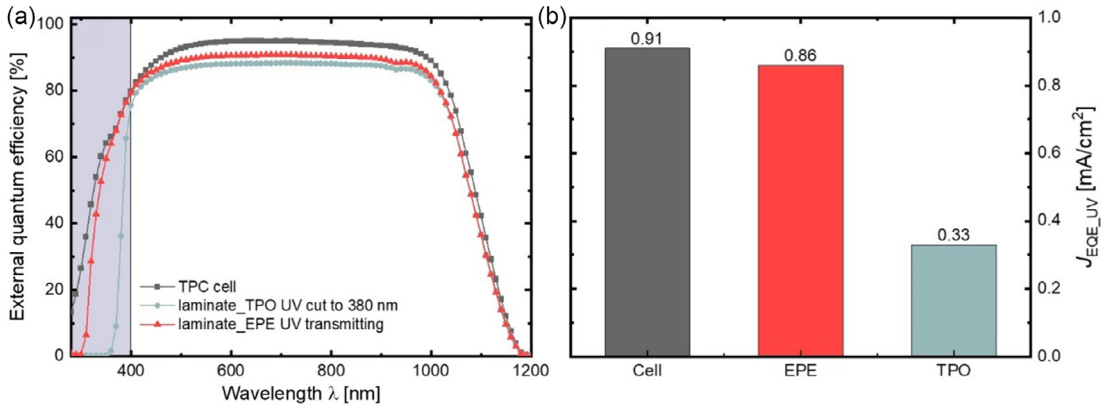

Figure 3. a) EQE of TPC cell, single-cell laminate utilizing UV-transmitting encapsulant (EPE) and single-cell laminate utilizing UV-cutoff encapsulant (TPO, UV cut to 380 nm). b) The integration current density generated by the UV light (280–400 nm) for the TPC cell and TPC singe-cell laminates using different encapsulants.

absorption. However, while a UV-transmitting encapsulation can preserve more of the current gain, the significant degradation issue may impede the adoption of TPC modules in the PV market. Therefore, in the pursuit of further enhancing the output of modules made of heterojunction solar cells, alternative solutions must be explored to address the dilemma between reducing parasitic absorption and ensuring UV stability of the module.

4. Alternative: UV-DS Encapsulant and Its OPAL2 Simulation

DC and DS processes have been extensively investigated in recent decades.[15,16,25,26] The widespread interest in the encapsulant developed on the basis of the DS mechanism is triggered by the urgent need to solve the UV-sensitivity problem of the SHJ module. This approach involves embedding DS materials in the PV encapsulant to convert the harmful UV light into visible light, which can then be absorbed and utilized by the solar cell. A concise overview of the DS process in the solar module is depicted in **Figure 4**. In the DS process, UV photons are initially absorbed by the DS materials dispersed in the encapsulant. Upon absorption, electrons within the DS materials are excited and temporarily remain in an excited state. Subsequently, the excited electrons undergo a non-radiative relaxation process, resulting in the reemission of a lower-energy photon with a longer wavelength than that of the absorbed UV photon.[16] During non-radiative relaxation, a phonon will be excited and some energy may be lost in the form of heat. Note that the reemission of photons is omnidirectional, meaning that not all of the converted visible light will be absorbed by the solar cell beneath the encapsulant. Furthermore, since the DS materials are only dispersed in the encapsulant, some of the UV light would not be absorbed and converted but would instead reach the surface of the solar cells. Overall, UV-DS encapsulation presents an ideal solution for the harmless utilization of light in the UV range of the AM 1.5G spectrum, offering promising prospects for the production of modules based on heterojunction solar cells.

To the best of our knowledge, the question of which kind of DS encapsulant is suitable for SHJ solar cells and its counterparts

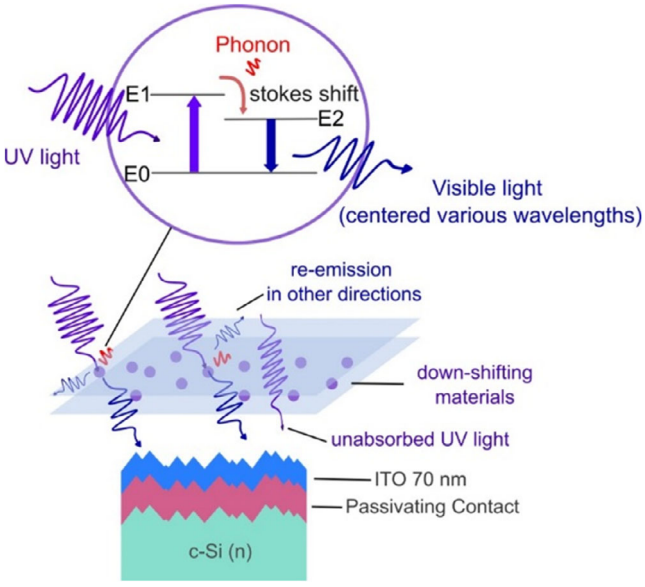

Figure 4. Sketch of function of the UV-downshifting encapsulant.

has not been answered yet. Here, we made an evaluation based on optical simulations, using OPAL2.[27] The methodology is a simplified way based on the spectral transfer matrix formalism,[18] which is depicted in **Figure 5**. For simplification, the DS process is imitated by varying the spectrum of photons radiated from the surface of solar cells. First, the AM 1.5G spectral irradiance was transformed into the spectral photon flux $\frac{d\Phi(\lambda)}{d(\lambda)}$, the photon flux per unit spectral width, according to

$$\frac{d\Phi(\lambda)}{d(\lambda)} = \frac{1}{h\upsilon}\frac{dW(\lambda)}{d(\lambda)} \quad (1)$$

where h is the Planck constant, υ is the radiation frequency, and $\frac{dW(\lambda)}{d(\lambda)}$ is the AM 1.5G spectral irradiance or power flux. The AM

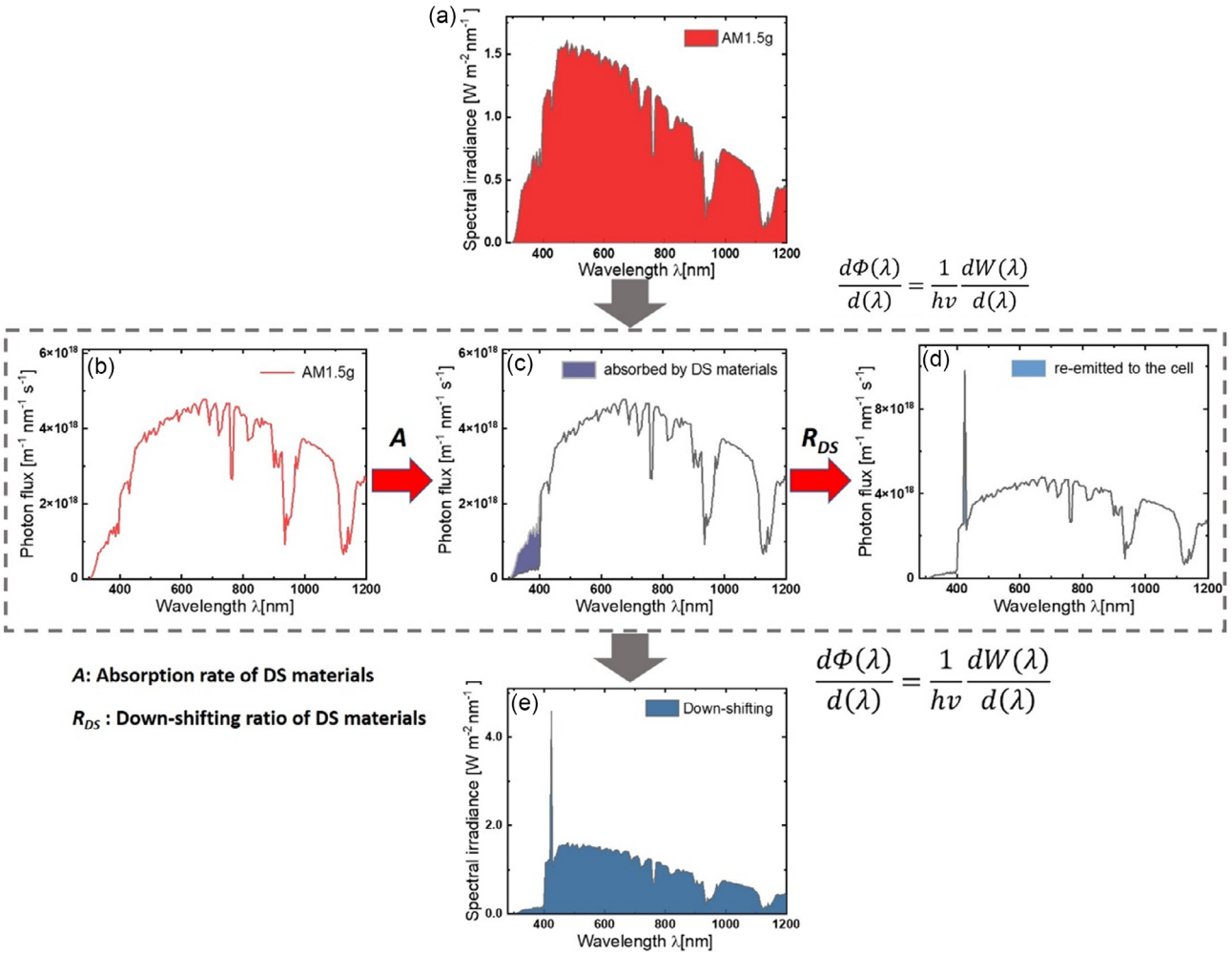

Figure 5. Work flow to mimic the process of downshifting for OPAL2 simulation. a) Irradiance spectrum and b) Photon flux spectrum at AM 1.5G. c) Diagram indicates the part of photon flux absorbed by DS materials (in purple) and d) Diagram indicates the part of photon flux down shifted and re-emitted to the cell (in light blue). e) Down-shifted irradiance spectrum.

1.5G spectrum and the transformed photon flux spectrum are shown in Figure 5a,b, respectively.

In the OPAL2 simulations, we need to input the spectrum of light irradiated on the surface of solar cells. Note that not all photons in the UV range from 280 to 400 nm are absorbed by the DS materials. In addition, the photons reemitted by the DS process would be emitted in all directions so there is an optical loss. Therefore, two factors must be considered. First, the absorption rate of DS materials needs to be defined. In this simulation, we set the percentage of UV photons absorbed by the DS materials (absorption rate, *A*) as 80%, based on the characteristics of the selected, commercially available UV-conversion foil.[28] The photon flux spectrum after applying the absorption rate is shown in Figure 5c. Second, we defined the DS ratio (R_{DS}), which represents the ratio of reemitted photons that reach the cell surface. R_{DS} in this simulation are set at 50%, 60%, and 70%. The reason for varying the R_{DS} around 60% was due to an estimation based on the EQE spectrum of the SHJ single-cell laminate using DS-EPE encapsulant, which is shown in Figure S3, Supporting Information. We found that the EQE curve in the UV range was similar to that in Figure 2a shown in ref. [20], of which the total DS efficiency was calculated at about 63%. The total DS efficiency was defined as a modified photoluminescence efficiency where various optical losses in the DS layer were taken into consideration. This factor resembles the R_{DS} here. To simplify the simulation process, we fix the spectral width of the reemitted photons to around 5 nm. This allows us to consider a scenario where UV light is converted into narrow-band visible light. In this way, the spectral photon flux at AM 1.5G is modulated to the customized DS photon irradiance, as depicted in Figure 5d. The final step is to transform the spectrum back to spectral irradiance, shown in Figure 5e, which is the form to enter into the OPAL2 simulation.

Figure 6 shows the simulated photon current generated in the substrate, J_G, of heterojunction solar cells with different front passivating contact structures. Herein, we simulated three types of contact structures, a-Si:H(n)/a-Si:H(i), nc-SiO_x:H(n)/a-Si:H(i), and nc-SiC:H(n)/SiO_x. These structures represent the mainstream SHJ structure, the cell design of the current world record

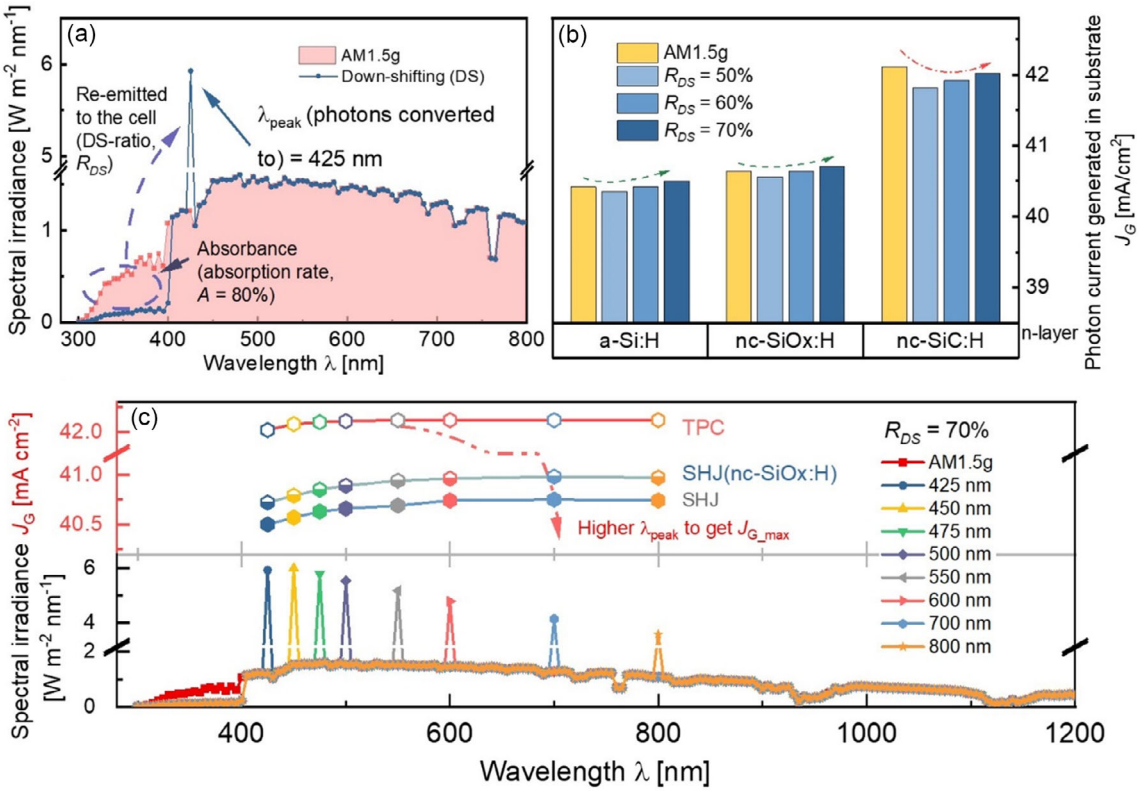

Figure 6. a) Customized DS spectrum input in OPAL2 for the simulation of DS encapsulant with various DS ratios (R_{DS}). Simulated photon current generated in the substrate (J_G) of heterojunction solar cells encapsulated by DS encapsulant b) with R_{DS} varied from 50% to 70% and c) with DS spectrum centered at different wavelength, from 425 to 800 nm.

holder, and potential candidates, respectively. The thickness of the ITO was fixed at 70 nm for lateral comparison of the performance of these cells with DS encapsulant. The transition from a-Si:H to nc-SiC:H involves the adoption of more transparent materials aimed at reducing parasitic absorption. This means that varying amounts of short-wavelength photons would reach the substrate for the different investigated structures. The comparison between these three contact structures allows investigating the question whether the application of a DS encapsulant contradicts the optical benefit of more UV-transparent front layers or how efficient the DSed light leads to improved carrier generation in SHJ solar cells. We simulated the reemission process by adjusting the R_{DS} of the DS encapsulant. Throughout this simulation, the peak of the DS spectrum, λ_{peak}, was maintained at 425 nm. As depicted in Figure 6a, following the absorption of 80% of photons in the UV range, 50–70% of these photons are reemitted onto the surface of solar cells. In Figure 6b, a comparison between the J_G under the AM 1.5G condition and under conditions of DS encapsulants with varied R_{DS} is presented. Similarly, when using an encapsulant with a relatively low R_{DS}, the gain triggered by DS fails to compensate for the current loss resulting from the reemission process. A higher R_{DS} is therefore necessary for all types of solar cells. In the case of a λ_{peak} of 425 nm, R_{DS} of 60% can fully counteract the negative impact of photon reemission on cells using a-Si:H(n) and nc-SiO$_x$:H(n). Further increases in the R_{DS} demonstrate a positive enhancement to the current. However, regarding nc-SiC:H(n)-based TPC cells, even with the highest simulated R_{DS} of 70%, the current still falls behind the case without DS encapsulant. Therefore, the problem of greater current loss arises when DS encapsulants are combined with more transparent front contacts. This is consistent with our observation of current enhancement in the UV range in TPC cells. These results suggest that the characteristic of the DS encapsulant should be optimized for different front passivating contacts of heterojunction solar cells. We systematically adjusted the λ_{peak} of the DS spectrum from 425 to 800 nm while maintaining the R_{DS} at 70%. Subsequently, the modulated spectra were applied to various cell structure simulations. Figure 6c presents the simulated results. It is evident that the maximum effects of DS encapsulants depend on the combination of the λ_{peak} of the encapsulant and the specific contact structure. For cell designs, a redshift of the wavelength range of the reemitted light is beneficial for current enhancement. Compared to TPC, a higher λ_{peak} is required to approach the maximum J_G for SHJ cells using the conventional a-Si:H(n) layer and the nc-SiO$_x$:H(n) layer. The maximum J_G at 700 nm of SHJ (a-Si:H(n)) is 40.75, 0.25, and 0.33 mA cm^{-2} higher than that with a λ_{peak} of 425 nm or AM 1.5G, respectively. In addition, the highest J_G of SHJ (nc-SiO$_x$:H(n)) is also achieved at the DS spectrum centered at 700 nm, which is 40.98, 0.27, or 0.34 mA cm^{-2} higher than that with a λ_{peak} of 425 nm or AM 1.5G, respectively. It demonstrates that the combination of

UV-DS encapsulant can further increase the output current of the SHJ-based module. The DS effect converts high-energy UV photons into lower-energy photons where the parasitic absorption of a-Si:H is reduced, which can be easily imaged based on the absorption coefficient curve of a-Si:H.[5] In the case of TPC, the DS process reemitted light with a spectrum centered at 550 nm can generate a J_G of 42.12 mA cm^{-2}. Although this value is just slightly higher than that of the AM 1.5G case, it underscores the capability of DS encapsulation to address the UVID problem for TPC cells without introducing current loss.

5. Conclusion

This work presents the UV-induced performance reduction occurring in SHJ solar cells and TPC solar cells. A significant decrease in V_{OC} and FF resulting from UV exposure was observed in TPC solar cells. This implies an urgent need to mitigate UVID not only in terms of conventional SHJ cell structure but also in cells featuring advanced concepts like TPC. A straightforward approach to circumvent this issue involves the integration of UV-modulation encapsulation during the module fabrication. However, EQE comparisons between TPC-based laminates with UV-cutoff encapsulant and UV-pass encapsulant point out the issue of current loss. This indicates that the UV-cutoff encapsulation can prevent the UV light from reaching the cell surface but the loss of current generated by the UV light significantly weakens the advantage of TPC cells, particularly their large current gain in the UV range. Therefore, normal UV-cutoff encapsulation is not the ideal option.

We propose to apply UV-DS encapsulants to mitigate the UVID and reduce the current loss in the encapsulation process. An evaluation based on optical simulations using OPAL2 was conducted. Different kinds of front passivating contacts, a-Si:H(n)/a-Si:H(i) stacks, nc-SiO$_x$:H/a-Si(i) stacks, and nc-SiC:H/SiO$_x$ stacks, were taken into consideration. The function of DS encapsulants is emulated by modulating the AM 1.5G spectral irradiance approaching the cell surface. Simulation results show that two factors influence the integration of DS encapsulants. One factor is the DS ratio (R_{DS}), which determines the amount of photons reemitted to the surface of cells. The other factor is the wavelength at which the down-converted photons are centered, defined as the λ_{peak}. A higher R_{DS} can compensate for more current losses in the DS process. In the case of SHJ cell, including both the conventional structure and the one utilizing nc-SiO$_x$, a DS encapsulant with a λ_{peak} at 425 nm and R_{DS} above 60% is enough to achieve higher current output than the cell under the AM 1.5G spectrum. However, for TPC solar cells, where the current enhancement mainly occurs in the UV range, a larger λ_{peak} is required to compensate for the current loss related to the DS process. Simulations varying λ_{peak} suggest the minimal wavelength that the DS encapsulant should reach to achieve the optimal current gain for all three types of solar cells. For TPCs, a shorter λ_{peak} at 550 nm is required to reach the maximal current generated in the substrate, J_G. Note that the current gain compared with the case of AM 1.5G is quite small, but the simulation demonstrates that the TPC concept and DS method can contribute together to the current gain of solar modules. Larger current gains were observed in the case of the other solar cells, but the λ_{peak} should also be longer, at 700 nm, to achieve the highest photon current generated in the substrate (J_G). The current gain from DS encapsulation is more obvious when it is applied to the solar cells with a-Si:H(n)/a-Si:H(i) stack or nc-SiO$_x$:H/a-Si(i) stack, which is 0.33 and 0.34 mA cm^{-2}, respectively.

6. Experimental Details

Fabrication of SHJ and TPC Solar Cells: The solar cells were fabricated on quartered M2$^+$-sized Czochralski grown n-type 1 Ω cm silicon <100> wafers supplied by LONGi. After the standard saw damage removal and texturization process, a DIO_3 cleaning process was performed, followed by native oxide removal in diluted 1% hydrofluoric acid (HF) for 5 min. For TPC cells, a roughly 1 nm thick wet-chemical SiO$_x$ was prepared on wafers in the Piranha solution consisting of H_2O_2 and H_2SO_4 with a ratio of 2:1, self-heated to ≈60 °C for 10 min before the deposition of thin-film layers. The a-Si:H layers for all cells, both sides of SHJ cells and the rear side of TPC cells, were deposited in a Meyer Burger AK1000 plasma-enhanced chemical vapor deposition (PECVD) system. The nc-SiC:H(n) layers for TPC cells were deposited by the MRG HWCVD system. Details of the HWCVD process can be found elsewhere.[5] For the TPC cell, the SiO$_x$ on the rear side of the wafer was removed by a HF dip process for 5 min before the deposition of the rear a-Si:H layers. And, 70 nm ITO layers were sputtered on both sides from a rotational target at 250 °C, with a sputtering power of 5 kW and a deposition pressure of 3 μbar. The active area of solar cells developed on wafers was defined by the ITO sputtered through a shadow mask with four 2×2 cm^2 openings. The Ag contacts were screen-printed by a Microtec MT-650TVC screen printer using a low-temperature silver paste supplied by NAMICS. Afterward, the silver paste was dried at 150 °C for 10 min and cured at 170 °C for 40 min. The post-treatment process on solar cells was carried out in the GSOLA GLR-4Z light-soaking system at 175 °C for 90 s.

TPC Laminates Preparation: The encapsulation structure in this investigation was glass/encapsulant/TPC cell/encapsulant/back sheet. The thickness of the glass was 3.2 mm. The transmittance of the sample can be found in Figure S1, Supporting Information. TPO and EPE were used as the encapsulant films for comparison. The back sheet was a PO-based foil. The TPC cell for the laminate was one piece (2.2×2.2 cm^2, with 2×2 cm^2 sized subcell) which was cut from the wafer by an in-house built laser-cutting system. Before lamination, the cell was connected using multiwire interconnection technology of coated wires with PO as the carrier foil. Sn–Pb-coated Cu ribbons were used as connectors. The vacuum lamination processes for TPO and EPE samples were carried out at the same pressure of 750 mbar, with the same evacuating time of 240 s and lamination time of 600 s. The only difference was the temperature. The lamination temperature was 150 and 155 °C for TPO and EPE samples, respectively. Transmittance and reflectance of the encapsulants were measured by a Perkin Elmer Lambda 950 UV–vis spectrophotometer, as shown in Figure S2, Supporting Information.

UV Exposure Testing Setup: UV exposure experiments were carried out in the lab of SHJ solar and module manufacturer, Anhui Huasun Energy Co., Ltd. The UV light source simulator was with ultraviolet A + ultraviolet B (UVA + UVB) irradiance set to an intensity of 200 W m^{-2}. The UVB (280–320 nm) content was around 5.9% of the total spectral irradiance. After 300 h of exposure, the cumulative UV irradiance was equivalent to a UV dose of 60 kWh m^{-2}. The temperature of the UV chamber was kept at 60 °C. A comparison between the spectrum of the UV light source and that of the sun (in the UVA + UVB range) can be found in Figure S6, Supporting Information.

Device Characterization: The PV parameters (V_{OC},J_{SC}, FF, and efficiency) of SHJ and TPC solar cells were measured by current–voltage (*I–V*) measurements under standard test condition (AM 1.5G, 25 °C, 1000 W m^{-2}). The EQE and the integral reflectance were measured with monochromatic illumination and an integrating sphere. All of these measurements were integrated in the LOANA solar cell analysis system from PV tools.

OPAL2 Simulation: Optical simulations were performed using OPAL2.[27] This optical simulator targeted the optical losses related to the front surface of solar cells. It calculated the reflection, absorption in the front thin-film layers, and the transmission into the substrate according to the user-defined front structure. According to the customized or given incident spectrum, the approximation of the photocurrent generated within the cell could be calculated. Three kinds of front structures were simulated in this work. More details of the parameters input in the simulation can be found in Supporting Information.

Supporting Information

Supporting Information is available from the Wiley Online Library or from the author.

Acknowledgements

The authors thank the support from B. Zwaygardt, A. Doumit, H. Siekmann, V. Lauterbach, A. Mück, and S. Lynen for laser cutting, cleaning, and texturing of wafers, depositions of a-Si:H and ITO layer, metallization, and light-soaking treatment. The authors also thank J. Wolff and A. Schmalen for the maintenance of HWCVD systems. This work was supported by the Helmholtz Nano Facility funded by the Helmholtz Association.[29] B.X. thanks to the financial support by the China Scholarship Council (CSC).

Conflict of Interest

The authors declare no conflict of interest.

Author Contributions

Binbin Xu: Conceptualization: (equal); Data curation: (lead); Formal analysis: (lead); Investigation: (lead); Methodology: (equal); Software: (equal); Validation: (equal); Visualization: (lead); Writing—original draft: (lead); Writing—review & editing: (lead). **Karsten Bittkau**: Conceptualization: (equal); Formal analysis: (equal); Methodology: (lead); Project administration: (equal); Software: (supporting); Supervision: (supporting); Validation: (equal); Visualization: (supporting); Writing—review & editing: (supporting). **Alexander Eberst**: Formal analysis: (supporting); Methodology: (supporting); Visualization: (supporting); Writing—review & editing: (supporting). **Kai Zhang**: Formal analysis: (supporting); Investigation: (supporting); Methodology: (supporting); Visualization: (supporting); Writing—review & editing: (supporting). **Yanxin Liu**: Methodology: (supporting); Validation: (equal); Writing—review & editing: (supporting). **Jinli Yang**: Investigation: (supporting); Resources: (supporting); Validation: (supporting); Writing—review & editing: (supporting). **Weiyuan Duan**: Resources: (supporting); Validation: (supporting); Writing—review & editing: (supporting). **Muhammad Ainul Yaqin**: Investigation: (supporting); Visualization: (supporting); Writing—review & editing: (supporting). **Vladimir Smirnov**: Writing—review & editing: (supporting). **Chunlan Zhou**: Writing—review & editing: (supporting). **Wenjing Wang**: Writing—review & editing: (supporting). **Xiaohua Xu**: Resources: (supporting). **Andreas Lambertz**: Conceptualization: (supporting); Investigation: (supporting); Methodology: (supporting); Project administration: (supporting); Supervision: (supporting); Writing—review & editing: (supporting). **Uwe Rau**: Methodology: (supporting); Supervision: (lead); Writing—review & editing: (supporting). **Kaining Ding**: Conceptualization: (lead); Funding acquisition: (lead); Investigation: (supporting); Methodology: (supporting); Project administration: (lead); Resources: (equal); Supervision: (equal); Validation: (equal); Visualization: (supporting); Writing—review & editing: (supporting).

Data Availability Statement

The data that support the findings of this study are available from the corresponding author upon reasonable request.

Keywords

downshifting encapsulations, optical simulations, silicon heterojunctions, transparent passivating contacts, ultraviolet-induced degradations

Received: July 25, 2024
Revised: October 18, 2024
Published online: November 5, 2024

[1] SolarPower Europe, *Global Market Outlook for Solar Power 2023–2027*, Solar Power Europe, Brussels, Belgium **2023**.
[2] Y. Zhao, P. Procel, C. Han, L. Cao, G. Yang, E. Özkol, A. Alcañiz, K. Kovačević, G. Limodio, R. Santbergen, A. Smets, A. Weeber, M. Zeman, L. Mazzarella, O. Isabella, *Sol. Energy Mater. Sol. Cells* **2023**, *258*, 112413.
[3] Z. Sun, X. Chen, Y. He, J. Li, J. Wang, H. Yan, Y. Zhang, *Adv. Energy Mater.* **2022**, *12*, 2200015.
[4] H. Lin, M. Yang, X. Ru, G. Wang, S. Yin, F. Peng, C. Hong, M. Qu, J. Lu, L. Fang, C. Han, P. Procel, O. Isabella, P. Gao, Z. Li, X. Xu, *Nat. Energy* **2023**, *8*, 789.
[5] M. Köhler, M. Pomaska, P. Procel, R. Santbergen, A. Zamchiy, B. Macco, A. Lambertz, W. Duan, P. Cao, B. Klingebiel, S. Li, A. Eberst, M. Luysberg, K. Qiu, O. Isabella, F. Finger, T. Kirchartz, U. Rau, K. Ding, *Nat. Energy* **2021**, *6*, 529.
[6] Y. Zhao, L. Mazzarella, P. Procel, C. Han, F. D. Tichelaar, G. Yang, A. Weeber, M. Zeman, O. Isabella, *Prog. Photovolt. Res. Appl.* **2022**, *30*, 809.
[7] D. Qiu, A. Lambertz, W. Duan, L. Mazzarella, P. Wagner, A. B. Morales-Viches, G. Yang, P. Procel, O. Isabella, B. Stannowski, K. Ding, *Adv. Sci.* **2024**, 2403728.
[8] A. Sinha, J. Qian, S. L. Moffitt, K. Hurst, K. Terwilliger, D. C. Miller, L. T. Schelhas, P. Hacke, *Prog. Photovolt. Res. Appl.* **2023**, *31*, 36.
[9] H. Ye, S. Huang, C. Qian, Z. Sun, Y. Chen, X. Song, Y. Zhang, N. Wang, Y. Hu, Y. Yang, L. Li, Z. Ma, T. Chen, W. Liu, J. Yu, *Sol. RRL* **2023**, *7*, 2300334.
[10] N. Pinochet, R. Couderc, S. Therias, *Prog. Photovolt. Res. Appl.* **2023**, *31*, 1091.
[11] G. Brito-Santos, B. Gil-Hernández, C. Hernández-Rodríguez, B. González-Díaz, R. Guerrero-Lemus, J. Sanchiz, *Mater. Sci. Eng. B* **2023**, *288*, 116207.
[12] Z. Yang, Y. Li, J. Wu, Y. Zheng, X. Fan, T. Bian, S. V. Masendu, R. Anton, J. Xu, B. Huang, Y. Fan, Z. Shao, *Sol. Energy Mater. Sol. Cells* **2023**, *257*, 112373.
[13] C. Jiang, G. Zhang, Z. Hong, J. Chen, Y. Li, X. Yuan, Y. Lin, C. Yu, T. Wang, T. Song, Y. Wang, B. Sun, *Adv. Mater.* **2023**, *35*, 2208042.
[14] C. Wu, S. Zou, C. Peng, S. Gu, M. Ni, Y. Zeng, H. Sun, X. Zhang, X. Su, *J. Energy Chem.* **2023**, *81*, 212.
[15] B. S. Richards, *Sol. Energy Mater. Sol. Cells* **2006**, *90*, 1189.
[16] X. Huang, S. Han, W. Huang, X. Liu, *Chem. Soc. Rev.* **2013**, *42*, 173.
[17] L. Prönneke, G. C. Gläser, U. Rau, *EPJ Photovolt.* **2012**, *3*, 30101.
[18] G. C. Glaeser, U. Rau, *Thin Solid Films*, **2007**, *515*, 5964.
[19] B. Lipovšek, A. Solodovnyk, K. Forberich, E. Stern, J. Krč, C. J. Brabec, M. Topič, *Opt. Express* **2015**, *23*, A882.
[20] R. Rothemund, *Sol. Energy Mater. Sol. Cells* **2014**, *120*, 616.
[21] T. Uekert, A. Solodovnyk, S. Ponomarenko, A. Osvet, I. Levchuk, J. Gast, M. Batentschuk, K. Forberich, E. Stern, H. Egelhaaf, C. J. Brabec, *Sol. Energy Mater. Sol. Cells* **2016**, *155*, 1.

[22] L. E. Black, K. R. McIntosh, *IEEE Trans. Electron Devices* **2010**, *57*, 1996.
[23] H. Sai, H. Hsu, P. Chen, P. Chen, T. Matsui, *Phys. Status Solidi A* **2021**, *218*, 2000743.
[24] V. Fiandra, L. Sannino, C. Andreozzi, G. Flaminio, M. Pellegrino, *Polym. Degrad. Stab.* **2024**, *220*, 110643,
[25] T. Trupke, M. A. Green, P. Würfel, *J. Appl. Phys.* **2002**, *92*, 1668.
[26] D. Verma, T. O. Saetre, O.-M. Midtgård, in *38th IEEE Photovoltaic Specialists Conf.*, IEEE, Piscataway, NJ **2012**, pp. 002608–002613.
[27] K. R. McIntosh, S. C. Baker-Finch, in *38th IEEE Photovoltaic Specialists Conf.*, IEEE, Piscataway, NJ **2012**, pp. 000265–000271.
[28] https://en.cybrid.com.cn/product_detail/101.html (accessed: May 2024).
[29] W. Albrecht, J. Moers, B. Hermanns, *J. Large Scale Res. Facil.* **2017**, *3*, A112.